Centro Euro-Mediterraneo sui Cambiamenti Climatici

Technical Notes
November 2020
Issue TN0289

ODA – Ocean modeling and Data Assimilation Division

Bulk Formulations in NEMOv.4: algorithms review and sea surface temperature response in ORCA025 case study

By **Giulia Bonino**
Fondazione CMCC Centro Euro-Mediterraneo sui Cambiamenti Climatici
giulia.bonino@cmcc.it

Doroteaciro Iovino
Fondazione CMCC Centro Euro-Mediterraneo sui Cambiamenti Climatici
dorotea.iovino@cmcc.it

Simona Masina
Fondazione CMCC Centro Euro-Mediterraneo sui Cambiamenti Climatici
simona.masina@cmcc.it

SUMMARY This report presents a review of the bulk formulae used to compute air-sea exchanges in the ocean model NEMOv4.0, and it describes the impact of the bulk formulations on the sea surface temperature simulated in the CMCC global configuration of the model at eddy permitting resolution.

DOI: https://doi.org/10.25424/cmcc/bulk_formulas_nemo_report

CONTENT

1. INTRODUCTION

The ocean interacts with the atmosphere via exchanges of momentum, heat and mass. These air-sea exchanges constitute the ocean-surface energy and water budgets, define the ocean's role in Earth's climate and its variability on both short and long timescales. Their knowledge is essential at suitable spatial and temporal scales in understanding and modeling several physical processes spanning various scales of atmospheric and oceanic motions. Direct flux measurements over the sea are available only at limited locations. In numerical ocean modeling, air-sea fluxes are commonly estimated from bulk flux parameterization using flux-related near-surface meteorological variables (wind speed, sea and air temperatures, and humidity). The development of accurate flux parameterizations has been a goal of airâsea interaction research for many decades.

In the NEMO ocean general circulation model [1], the air-sea turbulent fluxes can be provided trough three different formulations: the analytical formulation, the flux formulation and bulk formulae formulation. Specifically, according to the analytical formulation all the turbulent fluxes are assumed to be uniform in space, while the flux formulation imposes that the fluxes needed are directly read from input files. Lastly, the bulk formulae formulation implies that the air-sea turbulent fluxes are computed using the sea surface properties and atmospheric surface state variables at height z above the sea surface. The traditional aerodynamic bulk formulas are:

$$\tau = \rho C_d u u_z \tag{1a}$$

$$Q_H = \rho C_p C_t (\theta_z - \theta_0) u \tag{1b}$$

$$E = \rho C_q (q_0 - q_z) u \tag{1c}$$

$$Q_L = -L_v E \tag{1d}$$

where τ is the wind stress, Q_H is the turbulent flux of sensible heat , E is the evaporation, and Q_L is the turbulent flux of latent heat. Throughout this report, a positive sign of τ , Q_H, and Q_L means a gain of the relevant quantity for the ocean. The term ρ is the density of air; C_d, C_t, and C_q are the Bulk Transfer Coefficients (BTCs) for momentum, sensible heat, and moisture, respectively; C_p is the heat capacity of moist air, and L_v is the latent heat of vaporization. u_z is the wind speed vector at height z. The bulk scalar wind speed u is the scalar wind speed $|u_z|$ with the potential inclusion of a gustiness contribution (see Bulk algorithm section in this report). θ_z and q_z are the potential temperature and specific humidity of air at height z, while θ_0, q_0 are he potential temperature and saturation-specific humidity at surface. Specifically, θ_z is defined as:

$$\theta_z = T_z + \gamma z \tag{1e}$$

where T_z is the temperature of air at height z and γz is a temperature correction term, which accounts for the adiabatic lapse rate and approximates the potential temperature at height z. q_z is defined as:

$$q_z = q_{sat}(d_z, SLP) \tag{1f}$$

The term d_z is the dew temperature, while SLP is the mean sea level pressure. q_0 is defined as:

$$q_0 = 0.98 q_{sat}(\theta_0, SLP) \tag{1g}$$

q_0 includes a 2% reduction to account for the presence of salt in seawater [2]. $q_{sat}(T, SLP)$, where T indicates d_z for q_z and θ_0 for q_0, is defined as:

$$q_{sat}(T, SLP) = \frac{\epsilon e_{sat}(T)}{SLP - (1-\epsilon) e_{sat}(T)} \tag{1h}$$

where $\epsilon = 0.62$ and $e_{sat}(T)$is calculated with the Goff-Gratch formula [3], as recommended by the World Meteorological Organization (WMO).

$$\begin{aligned} \log_{10}(e_{sat}(T)) = {} & 10.79574(1 - T_0/T) \\ & - 5.028 \log_{10}(T/T_0) \\ & + 1.5047510^{-4}[1 - 10^{-82969(T/T_0 - 1)}] \\ & + 0.4287310^{-3}[10^{4.76955(1-T_0/T)} - 1] \\ & + 0.78614, \end{aligned} \tag{1i}$$

where T_0 is the Triple point of freshwater (273.16 K). Depending on the bulk parameterization used, θ_0 can be the temperature at the air-sea interface (sea surface skin temperature, SSST or T_s) or at a few tens of centimeters below the surface (sea surface temperature, SST). The SSST differs from the SST due to the contributions of two effects of opposite sign: the cool skin and warm layer (CSWL). The cool skin is millimeter-scale uppermost layer of the ocean where a vertical gradient of temperature exists to sustain the heat flux continuity between ocean and atmosphere. The warm layer is the warming of the upper few meters of the ocean under day and sunny conditions. Figure 1 summarizes the bulk formulae approach implemented in the Ocean Global Circulation Model (adapted from Brodeau et al. 2017 [4]). Bulk algorithms differ in how they parametrize the exchange coefficients.

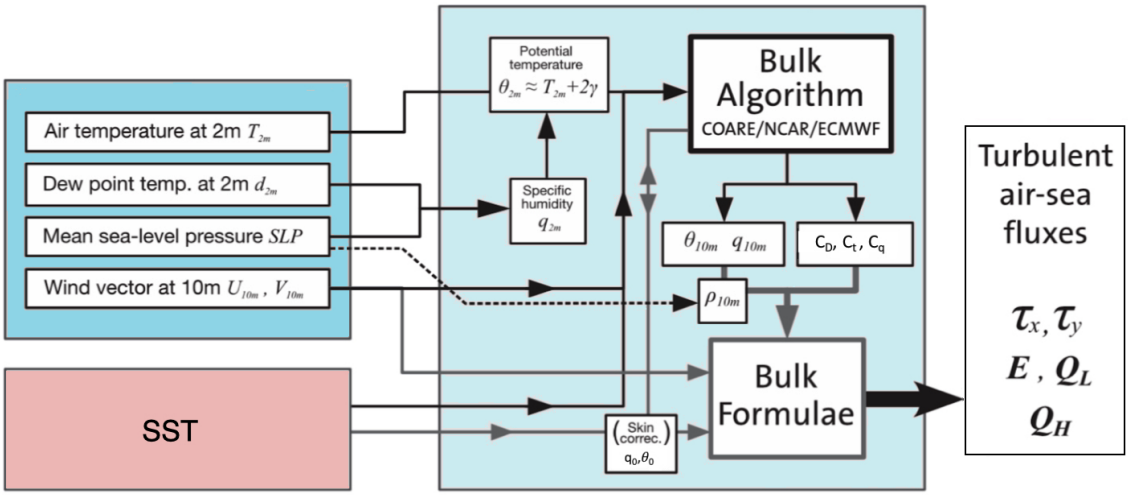

Figure 1: Bulk methodology for the computation of turbulent air-sea fluxes based on the sea surface and near-surface atmospheric state variables. Note that T and q are not always provided at the same height as the wind speed (usually 2 and 10 m, respectively). Therefore, prior to using bulk formulas (Equation 1), u and q are adjusted to the standard 10m height of during the computation of transfer coefficients (in the bulk algorithm). Figure modified from Brodeau et al. 2017. [4]

Here, we focus on three algorithms implemented in the most recent release of NEMO ocean model (v.4 revision 12050): COARE3.6 (Edson et al. 2013, [5]), NCAR (following Large and Yeager 2009 [6]), and ECMWF as the version of the bulk algorithm used in the recent cycles of the Integrated Forecast System (IFS) developed at ECMWF, such as cycle 41 (ECMWF, 2015 [7]). The purpose of the report is to review these bulk formulas and to discuss their impacts on sea surface temperature (SST). In particular, we highlight bulk algorithms similarities and differences in parametrizing the bulk transfer coefficients and we discuss the effect of these different parameterizations on sea surface temperature using the global NEMO at eddy-permitting configuration implemented at CMCC and generally identified as ORCA025. The report is organized as follow: in section 2, we provide a overview of the bulk formulas (2.1), some well-established bulk algorithms and the differences among them (2.2). In section 3, we present a set of numerical experiments performed with the newest version of the NEMO model (NEMOv4.0 revision 12050, [1]) in global configurations in order to study and to quantify the sea surface ocean response to the different bulk formulations. Section 4 presents the conclusions and the future perspectives.

2. THE BULK MODEL

In this section we present the bulk model theoretical background, the derivation of the Bulk Transfer Coefficients and the role of the roughness lengths and of the atmospheric stability (subsection 2.1). Then, we present the bulk algorithms implemented in NEMOv4.0 (subsection 2.2).

2.1 THEORETICAL BACKGROUND

1. **Derivation of C_D, C_t , C_q**

From Monin-Obukhov similarity theory (MOST, Monin and Obukhov 1954 [8]), the wind, the temperature and the specific humidity profiles in the atmospheric boundary layer can be defined as

$$u_z = u_0 + \frac{u_*}{k}[ln(\frac{z}{z_0}) - \varphi_m] \tag{2a}$$

$$\theta_z = \theta_0 + \frac{\theta_*}{k}[ln(\frac{z}{z_{0t}}) - \varphi_t] \tag{2b}$$

$$q_z = q_0 + \frac{q_*}{k}[ln(\frac{z}{z_{0q}}) - \varphi_q] \tag{2c}$$

$$\varphi_x = \varphi_x(\phi_x); \phi_x = \phi_x(\zeta); \zeta = \frac{z}{L} \tag{2d}$$

where z is the height above the ocean, z_0, z_0t, z_0q are called roughness lengths, K = 0.4 is the von Karman constant, while φ_m,φ_q,φ_q are the stability correction functions for the wind, temperature and moisture profiles, respectively. They depend on ϕ that, in turn, depends on the stability parameter ζ (Eq.2d, see stability function paragraph for further details). u_* is the scaling parameter for wind or friction, q_* the scaling parameters for humidity, θ_* the scaling parameter for potential temperature. They are characteristic velocity, humidity and potential temperature in the atmospheric boundary layer. First, we focus in the derivation of BTCs, while the stability parameters and the roughness lengths are discussed in the following paragraphs. Considering that the wind approaches zero near the coast (u_0=0), we can write the scaling parameters (u_*, q_*, θ_*) as

$$u_* = \frac{uk}{[ln(\frac{z_u}{z_0}) - \varphi_m]} \tag{3a}$$

$$\theta_* = \frac{(\theta_z - \theta_0)k}{[ln(\frac{z_t}{z_{0t}}) - \varphi_t]} \tag{3b}$$

$$q_* = \frac{(q_z - q_0)k}{[ln(\frac{z_q}{z_{0q}}) - \varphi_q]} \tag{3c}$$

The scaling parameters or turbulent scales can be defined from scaling/dimensional analysis of (1a),(1b) and (1c)

$$u_* = \sqrt{\frac{\tau}{\rho}}; \theta_* = \frac{Q_H}{\rho C_p u_*}; q_* = \frac{E}{\rho u_*} \tag{4}$$

Combining Eq. (4) with Eq.(1) yields

$$\rho u_*^2 = \rho C_d u^2; C_d = \frac{u_*^2}{u^2} \tag{5a}$$

$$\rho C_p u_* \theta_* = \rho C_p C_t (\theta_z - \theta_0) u; C_t = \frac{u_* \theta_*}{(\theta_z - \theta_0) u} \tag{5b}$$

$$\rho u_* q_* = \rho C_q (q_z - q_0) u; C_q = \frac{u_* q_*}{(q_z - q_0) u} \tag{5c}$$

Replacing the scaling parameters with Eq. (3), we obtain:

$$C_d = k^2[ln(\frac{z_u}{z_0}) - \varphi_m]^{-2} \tag{6a}$$

$$C_t = k^2[ln(\frac{z_u}{z_0}) - \varphi_m]^{-1}[ln(\frac{z_t}{z_{0t}}) - \varphi_t]^{-1} \tag{6b}$$

$$C_q = k^2[ln(\frac{z_u}{z_0}) - \varphi_q^{-1}[ln(\frac{z_t}{z_{0q}}) - \varphi_q]^{-1} \tag{6c}$$

Here z_u, z_t and z_q are the height above the surface for the wind, the potential temperature, and the specific humidity. In neutral condition (e.g. stability correction approaches to 0, $\varphi_m == 0$, $\varphi_t == 0$,$\varphi_q == 0$) at reference level (10m)

$$C_{dN} = k^2[ln(\frac{10}{z_0})]^{-2} \tag{7a}$$

$$C_{tN} = k^2[ln(\frac{10}{z_0})]^{-1}[ln(\frac{10}{z_{0t}})]^{-1} \tag{7b}$$

$$C_{qN} = k^2[ln(\frac{10}{z_0})]^{-1}[ln(\frac{10}{z_{0q}})]^{-1} \tag{7c}$$

The relations between the two are:

$$\sqrt{\frac{C_d}{C_{dN}}} = \frac{1}{1 + (\frac{C_{dN}}{k})[ln(\frac{z_u}{10}) - \varphi_m]} \tag{8a}$$

$$\frac{C_t}{C_{tN}} = \frac{\sqrt{\frac{C_d}{C_{dN}}}}{1 + (\frac{C_{tN}}{(k\sqrt{C_{dN}})})[ln(\frac{z_t}{10}) - \varphi_t]} \tag{8b}$$

$$\frac{C_q}{C_{qN}} = \frac{\sqrt{\frac{C_d}{C_{dN}}}}{1 + (\frac{C_{qN}}{(k\sqrt{C_{dN}})})[ln(\frac{z_q}{10}) - \varphi_q]} \tag{8b}$$

The BTCs are functions of stability parameter and roughness lengths (see more details in the following paragraphs).

2. **Stability parameters**

The stability functions defined as φ_m, φ_t,φ_q in Equations 2 are empirical function which depend on ϕ that in turns depends on ζ (Eq. 2d) which is called stability parameter and it is defined as $\zeta = \frac{z}{L}$. z is the height above the ocean and L is the Monin-Obukhov length. This length represents the height at which mechanically produced (by vertical shear) turbulence is in balance with the dissipative effect of negative buoyancy:

$$L = \frac{u_*^2\theta_v}{gk\theta_{v*}} \tag{9}$$

where θ_v is the virtual potential density defined as $\theta_v = \theta + 0.61q\theta$; while θ_{v*} is the the scaling parameter or turbulent scale for the virtual potential temperature $\theta_{v*} = \theta_*(1 + 0.61q_*)$
Physical interpretation:

(a) |L| is the height above the ground where the buoyancy and shear production of Turbulent Kinetic Energy (TKE) are of equal magnitude; below this height shear dominates and above it buoyancy dominates.

(b) The parameter θ_{v*} is proportional to $\theta_{v*}(z_u) - \theta_{v*}(z_0)$, the vertical difference in potential virtual temperature. The greater θ_v at z_0 in comparison with its value at z, the more negative the change in θ_v with increasing height, and the greater the instability of the surface layer. In such cases, L is negative but has a small magnitude, since it is inversely proportional to θ_{v*} when L is negative with a small magnitude, z/L is negative with a large magnitude. Such values of z/L correspond to large instability due to buoyancy. Positive values of z/L correspond to increasing θ_v with altitude and stable stratification.

Therefore, the function $\varphi(\phi)$ is the correction to the logarithmic wind profile resulting from the deviation from neutral stratification. Specifically, under neutral stability conditions, $z/L = 0$ and $\varphi(\phi)$ drops out; in stable conditions $z/L > 0$ and $\varphi(\phi) < 0$ and in unstable conditions $z/L < 0$ and $\varphi(\phi) > 0$.The universal function varies in different algorithms, nevertheless the one proposed by Paulson (1970) is widely accepted and gives a good fit to the data.

$$\varphi_m = 2ln(\frac{1-\phi_m^-1}{2}) + ln(\frac{1-\phi_m^-1}{2}) - tan^1\phi_m^-1 + \frac{\pi}{2} \quad \zeta < 0(\text{unstable}); \quad \varphi_m = 1 - \varphi_m \quad \zeta > 0(\text{stable}) \tag{9a}$$

$$\varphi_t = \varphi_q = 2ln(\frac{1-\phi_t^-1}{2}) \quad \zeta < 0(\text{unstable}); \quad \varphi_t = \varphi_q = 1 - \varphi_t \quad \zeta > 0(\text{stable}) \tag{9b}$$

Usually, it is ϕ that changes and in particular the α, β, γ coefficients.

$$\phi_m = \begin{cases} 1 + \gamma\zeta, & \zeta > 0 \text{ stable} \\ [1 - \alpha\zeta]^{-\beta}, & \zeta < 0 \text{ unstable} \end{cases} \quad \text{and} \quad \phi_t = \phi_q = \phi_m^2 \tag{10}$$

3. **Roughness lengths**

This parameter z_0, the integration constant, represents the height on which the mean wind speed calculated by Eq. (2) goes to zero. In reality, the wind at this height no longer follows a mathematical logarithm. Whilst it is not a physical length, it can be considered as a length-scale representation of the roughness of the surface. The roughness length is approximately one-tenth of the height of the surface roughness elements. Depending on z_0 the wind profile is different.

z_0 is usually defined as $z_0^{smooth} + z_0^{rough}$ where the first term relates to aerodynamically smooth surfaces on which the stress is exerted by viscosity and within the laminar sublayer (inversely proportional to wind); while the second term relates to rough surface where the effect of viscosity is negligible and it accounts for the actual roughness elements driven by the wind stress in the form of surface gravity waves. So the roughness length is given by

$$z_0 = \frac{0.11\nu}{u_*} + \frac{\alpha u_*^2}{g} \tag{11}$$

where ν is the kinematic viscosity of dry air, u_* is the the friction velocity, g is the gravitational acceleration and α is the Charnock coefficient, a dimensionless constant whose value varies with wind speed among the different algorithms, being fixed to 0.018 in ECMWF, or being a function of wind speed in COARE3.6. The z_{0t} and z_{0q} are roughness lengths corresponding to potential temperature and specific humidity. They differ in different algorithms and they are empirical or function of z_0.

2.2 BULK ALGORITHMS IN NEMOV.4

1. **ECMWF**

The ECMWF algorithm (ECMWF,2015 [7]) is implemented in the ECMWF Integrated Forecast System. The formulation takes advantage of the MOST theory. The computation of scalar wind speed includes the convective gustiness. The convective gustiness is a temporary increased of the wind speed due to the friction and the free convection. Gustiness in surface wind fields is assumed to arise in proportion to the intensity of convective precipitation. The algorithm considers the skin surface temperature in place of the SST, so that the CSWL scheme is included in the algorithm in order to compute the skin temperature from sea surface temperature. The algorithm parametrizes the roughness lengths. Indeed, in the unstable atmospheric surface layer, as the wind speed approaches zero, the production of TKE is dominated by buoyancy. Under such convective and calm conditions, standard bulk formulas are not suitable as they suggest that evaporation and turbulent heat fluxes tend to zero. These conditions were investigated in laboratory and model studies, which led to the addition of a parameterized convective gustiness contribution to the wind speed in the bulk algorithm. The algorithm consists in several iterations in order to make the results to converge. Before the iteration the algorithm provide first guess for u_*, q_*, θ_*. The principal equations to identify the coefficients in the iteration block are

$$u = \sqrt{u_*^2 + w_g}; \quad w_g = \beta w_*; \quad w_* = (-\frac{g}{\theta_*}\theta_{v*}u_* z_i)^{1/3}; \quad \theta_{v*} = -\frac{u_*^2\theta_v}{kgL} \tag{12}$$

u is the near-surface wind speed with the inclusion of convective gustiness (w_g), β is a coefficient and w_* is the convective velocity scale. L is is the Monin-Obukhov length (Eq. 9), g is the gravity, u_* is the scaling parameter for wind or friction, θ_v is the virtual potential temperature (Eq. 9), $\theta_{v*}$is the scaling parameter for virtual potential temperature (Equation 9) and z_i is the height of the atmospheric boundary layer.

The roughness parameters are defined as:

$$z_0 = \frac{\alpha\nu}{u_*} + \frac{\alpha u_*^2}{g}; \quad z_{0t} = \frac{0.40\nu}{u_*}; \quad z_{0q} = \frac{0.62\nu}{u_*} \tag{13}$$

The scaling parameters are then uploaded as

$$u_* = \frac{uk}{[ln(\frac{z_u}{z_0}) - \varphi_m]}; \quad \theta_* = \frac{(\theta_z - \theta_0)k}{[ln(\frac{z_t}{z_{0t}}) - \varphi_t]}; \quad q_* = \frac{(q_z - q_0)k}{[ln(\frac{z_q}{z_{0q}}) - \varphi_q]} \tag{14}$$

where

$$L = \frac{u_*^2\theta(1+0.61q)}{gk\theta_* + 0.01\theta_* q_*} \tag{15}$$

and

$$\phi_m = \begin{cases} 1+5\zeta, & \zeta > 0 \text{ stable} \\ [1-16\zeta]^{-1/4}, & \zeta < 0 \text{ unstable} \end{cases} \quad \text{and} \quad \phi_t = \phi_q = \phi_m^2 \tag{16}$$

Cd, Ct and Cq are then calculated using Eqs (6a), (6b), (6c)

2. **COARE3.6** The COARE3.6 [5] formulations are very similar to ECMWF algorithm (Pelletier et al. 2018 [9]). As the ECMWF bulk, it uses the Monin-Obukhov similarity theory and it takes in account the gustiness associated with convective situations. Furthermore, the algorithm considers the skin surface temperature in place of the SST, so that the CSWL scheme is included in the formulation. The algorithm differs from the ECMWF in the parametrization of the roughness lengths and for the stability empirical functions. The roughness lengths are

$$z_0 = \frac{0.11\nu}{u_*} + \frac{\alpha u_*^2}{g}; \quad \text{where } \alpha = \begin{cases} 0.11, & u_z < 10m/s \\ 0.11 + \frac{0.07}{8}(u-10), & 10m/s < u_z < 18m/s \\ 0.018, & u_z > 18m/s \end{cases} \tag{17}$$

$$z_{0q} = z_{0t} = min(1.1X10^{-4}, 5.5X10^{-5R_r^{-0.6}}) \quad \text{where } R_r = \frac{z_0 u_*}{\nu} \tag{18}$$

R_r is the roughness Reynolds number. α is equal to 0.018 and does not change as function of the wind speed. The stability empirical functions are given by

$$\phi_m = \begin{cases} 1+4.7\zeta, & \zeta > 0 \text{ stable} \\ [1-15\zeta]^{-1/4}, & \zeta < 0 \text{ unstable} \end{cases} \quad \text{and} \quad \phi_t = \phi_q = \phi_m^2 \tag{19}$$

3. **NCAR**

NCAR algorithm (Large and Yeager 2009 [6]) is based on field experiments showing that the C_{DN} tends to be a function only of the wind speed at reference level under the neutrally stable conditions (U_{10N}). They parameterize directly the neutral transfer coefficient:

$$C_{DN} = (aU_{10N}^{-1} + b + cU_{10N})x10^{-3} \tag{20a}$$

where the parameters a, b and c are determined by the field data. For the NCAR algorithm, a = 2.70, b = 0.142, and c = 0.76. When U_{10N} is infinitely small, C_{DN} is infinitely large, so a minimum Umin is usually set in the computation to avoid zero singularity. In particular, the zero wind singularity is avoided by simply setting a minimum value for the scalar wind speed of 0.5 m/s (no wind gustiness). The algorithm considers SST rather than skin surface temperature. The transfer coefficients for evaporation, Cq, and sensible heat, Ct are given as follows:

$$1000C_q = 34.6\sqrt{C_D} \tag{20b}$$

$$1000C_t = \begin{cases} 18.0\sqrt{C_D}, & \zeta > 0 \text{ stable} \\ 32.7\sqrt{C_D}, & \zeta < 0 \text{ unstable} \end{cases} \tag{20c}$$

Instead of parameterizing the roughness lengths, NCAR parametrized the neutral drag coefficient directly as functions of neutral wind speed. In contrast to other algorithms, while doing the iterations, the potential temperature, specific humidity and the wind data have to be shifted to 10m above the ocean and to neutral condition to use the above parametrizations. The algorithm consists in several iterations in order to make the results to converge. Before the iteration the algorithm provide first guess for u_*, t_*, q_* and transfer coefficients (using the equation above and considering $U_{10N} = u_z$). The principal equations to identify the coefficients in the iteration block consist in shifting of the wind, temperature and humidity (at height z_u, z_t and z_q) to 10m high and under neutral condition as follow.

$$U_N = |\Delta U| \quad (1 + \frac{\sqrt{C_D}}{k}[ln(\frac{z_u}{10}) - \varphi_m])^{-1} \tag{21a}$$

$$\theta_{10m} = \theta_{zt} - \frac{\sqrt{\theta_*}}{k}[ln(\frac{z_t}{10}) + \varphi_t(10m) - \varphi_t(z_t)] \tag{21b}$$

$$q_{10m} = q_{zq} - \frac{\sqrt{q_*}}{k}[ln(\frac{z_q}{10}) + \varphi_q(10m) - \varphi_q(z_q)] \tag{21c}$$

where

$$u_* = \sqrt{\rho_a^{-1}|\tau|} = \sqrt{C_D}|\Delta U| \tag{22a}$$

$$\theta_* = \frac{Q_H}{\rho_a C_p u_*} = \frac{C_t}{\sqrt{C_D}}[\theta_{zt} - \theta_0] \tag{22b}$$

$$q_* = \frac{E}{\rho_a u_*} = \frac{C_q}{\sqrt{C_D}}[q_{zt} - q_0] \tag{22c}$$

with stability parameters and functions as in the COARE3.6 algorithm (Equation 20a). Once the neutral 10m transfer coefficients are obtained from Equations 21, they are shifted to the measurement height (z_u) and stability using the relation between C_x and C_{xN} prensented in Eq. 8.

4. **Comparison among algorithms: Charnock parameter and Coefficients**

To calculate the BTCs, every bulk algorithm relies on an empirical closure. In algorithms such as COARE3.6 and ECMWF, as explained before (see Eq. 11), the roughness length z_0 is related to the friction velocity u_* [10]. In COARE3.6, the Charnock parameter is set to 0.006 in the range from 0 to 10 m/s, linearly increases from 0.006 to 0.028 in the range 10 and 18 m/s, and remains equal to 0.028 for higher wind speeds (Figure 2a). ECMWF algorithm relies on a fixed Charnock parameter equal to 0.018. The NCAR algorithm is based on a closure proposed by Large and Pond (1981,

1982), in which the three neutral BTCs are empirical functions of U_{N10}. As noted by Beljaars (1997) [11], 'neutral transfer coefficients and surface roughness lengths are compatible concepts' so that the $z_0(u_*)$ type of closure can be easily translated to the $C_D(U)$ type, such as:

$$C_D^{N10} = \frac{k^2}{[ln(\frac{10}{z_0})]^2}; \quad \alpha = \frac{g}{u_*^2}(10e^{-k/C_D^{N10}} - \frac{0.11\nu}{u_*}) \tag{23}$$

Similar to COARE3.6, the NCAR algorithm also suggests a roughly linear increase of α from moderate breeze to gale conditions, with a maximum value of 0.012 reached at a wind speed of about 25 m/s. The hurricane correction introduced in the latest update of the NCAR algorithm (Large and Yeager 2009) prevents the growth of C_D under very strong winds, which implies a decreasing value of αor winds above 25 m/s. Regarding the C_D transfer coefficient, the combination of the smooth-flow parameterization that increases with decreasing wind and a rough-flow parameterization that increases with increasing wind results in a minimum in the total roughness and BTCS. Kraus and Businger (1994) [12] predict that the roughness length and thereby the drag coefficient are expected to have a minimum for a wind speed between 2 and 3 m/s (Figure 2b). In particular, for wind speeds above 5 m/s , the C_D of NCAR is smaller than that of COARE3.6 and ECMWF. This leads to a substantial reduction of the wind stress : at the equator and over the ACC and northern midlatitudes, and Atlantic storm. From calm up to light breeze conditions (U10 , 5 m/s), the C_D of NCAR is larger than that of COARE3.6 and ECMWF. These conditions occur quite frequently particularly outside of the tropical band.

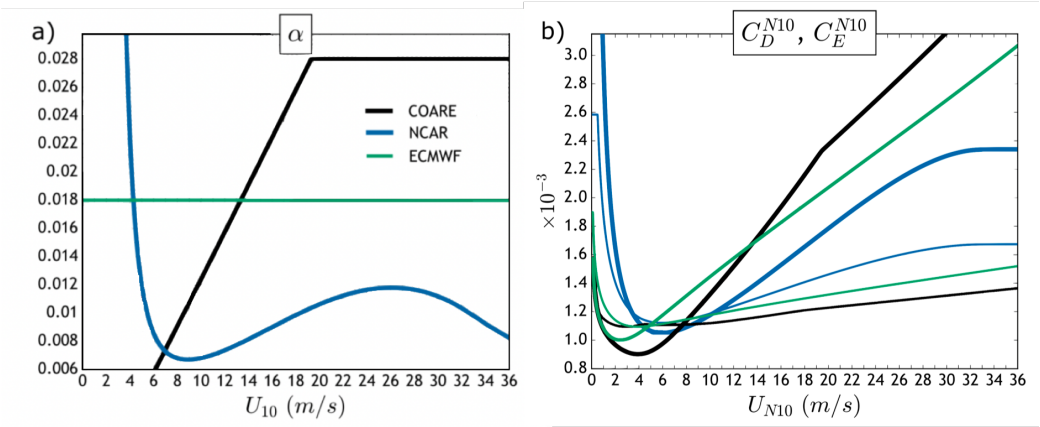

Figure 2: Bulk empirical closures as a function of the wind speed at 10 m for COARE(black), NCAR (blue), and ECMWF (green) bulk algorithms. (a) Charnock parameter a; for NCAR, a is calculated according to Eq. 12. (b) Neutral drag (C_D^{N10}) and moisture transfer coefficients (C_E^{N10}) (thick and thin lines, respectively), as functions of the neutral wind speed at 10 m. Figure modified from Brodeau et al. 2017. [4].

Table 1 summarizes the principal differences among algorithms. In details, skin surface temperature and convective gustiness are used in COARE and ECMWF algorithms, while NCAR uses SST and the zero wind singularity is avoided by simply setting a minimum value for the scalar wind speed of 0.5 m/s. Furthermore, ECMWF and COARE3.6 parametrize the roughness lengths, using the

Charnock parameter (α) , while NCAR uses the three neutral BTCs as empirical functions of U_{N10}. Lastly, the coefficients of the stability empirical function are the same for ECMWF and NCAR, while COARE3.6 adopts slightly different coefficients.

	Skin Temperature	Gustiness	Charnock (α)	Stability (Eq 10)
COARE3.6	yes	yes	$\alpha(U)$	$\alpha = 15; \beta = 1/4;$ γ=4.7
ECMWF	yes	yes	0.018	$\alpha = 16; \beta = 1/4;$ γ=5
NCAR	no	no ($u > 0.5m/s$)	not explicit (but $\alpha(U)$)	$\alpha = 16; \beta = 1/4;$ γ=5

Table 1: Principal differences among COARE3.6, ECMWF and NCAR algorithms.

3. SEA SURFACE TEMPERATURE RESPONSE TO BULK ALGORITHMS

This section presents the impact of the chosen bulk formulation on the simulated sea surface temperature. First, we present the set of experiments performed using the global NEMO-ORCA025 configuration, a global ocean/sea ice configuration at eddy-permitting resolution based on the ORCA025 grid (subsection 3.1), then we present some preliminary results (subsection 3.2). In particular, we describe the role of different atmospheric forcing (JRA55 and ERA5) and the contribution of the skin temperature in driving SST differences among set of experiments. Lastly, we discuss the potential role of the wind stress and the related transfer coefficient in effecting the sea surface temperature pattern.

3.1 EXPERIMENTS SET-UP

To discuss the ocean response to the different bulk formulations implemented in the new version of NEMO global ocean model (v.4, revision 12050, [1]), we performed four set of numerical experiments. The set differ for the forcing used (ERA5 or JRA55-do-v1.4) or for the implementation of the skin temperature in the bulk algorithms (SKIN [_S] or NOSKIN [_NS]). Each set consists in 3 simulations, all covering the period 2016-2018. 'Each simulation in the set differs for the bulk formula used to estimate air-sea fluxes (_ECMWF, _NCAR, _COARE3.6). The set of experiments are identified as:

1. **JRA55_NS** includes three experiments which differ for the bulk formulation used to estimate air-sea fluxes (ECMWF, NCAR, COARE3.6). All the experiments are forced by the surface-atmospheric dataset (version 1.4) for driving ocean-sea-ice models based on the Japanese 55-year Reanalysis [13] (hereinafter JRA55-do), the bulk algorithms do not include the skin temperature.

2. **ERA5_NS**: It consists in 3 experiments which differ for the bulk formulation used to estimate air-sea fluxes (ECMWF, NCAR, COARE3.6). All the experiments are forced by the ERA5 Reanalysis [14] (dataset from Copernicus Climate Change Service (C3S), 2017, [15]), and the bulk algorithms do not include the skin temperature.

3. **ERA5_S**: It consists in 3 experiments which differ for the bulk formulation used to estimate air-sea fluxes (ECMWF, NCAR, COARE3.6). All the experiments are forced by the ERA5 Reanalysis, the bulk algorithms include the Cool Skin Warm Temperature scheme (CSWL), except for NCAR algorithm. In contrast to COARE3.6 and ECMWF, the NCAR algorithm is calibrated and developed for the SST.

To analyze the impact of the experimental setup on the ocean state, we compare the model fields with the SST data product made available from National Oceanic and Atmospheric Administration with the Optimum Interpolation 0.25 Degree Daily SST Analysis data (Reynolds et al., 2007, [16]), hereafter referred to as NOAA SST

3.2 RESULTS

JRA55_NS VS ERA5_NS

In this subsection we present the differences in the mean SST between JRA55_NS and ERA5_NS set of experiments and we compare the simulated SST with NOAA SST. The role of the forcing in driving SST field is inferred from the SST differences of the experiments of each set with respect to NOAA SST (compare Figure 3a with Figure 3b). In the open ocean the two set of experiments, forced by the two reanalyses, present SST biases of opposite sign: the JRA55_NS warm biases are damped and turned in light cold biases, especially over Atlantic basin, in the ERA5_NS set. In both set of simulations, Eastern Boundary Upwelling Systems (EBUS, location of the most persistent biases in the OGCM) and Antarctica are warmer and Arctic ocean is colder compared to observations. On the other hand, the differences among experiments of each set (see Figure 4a or Figure 4b) teach us about the role of the bulks in shaping the sea surface ocean temperature. SST differences among experiments of JRA55_NS and ERA5_NS present the same pattern: ECMWF SST results colder than NCAR and COARE3.6 SST over EBUS and over equatorial Pacific and Atlantic, with a maximum value up to $0.6°C$. The discrepancy is, therefore, forcing independent.

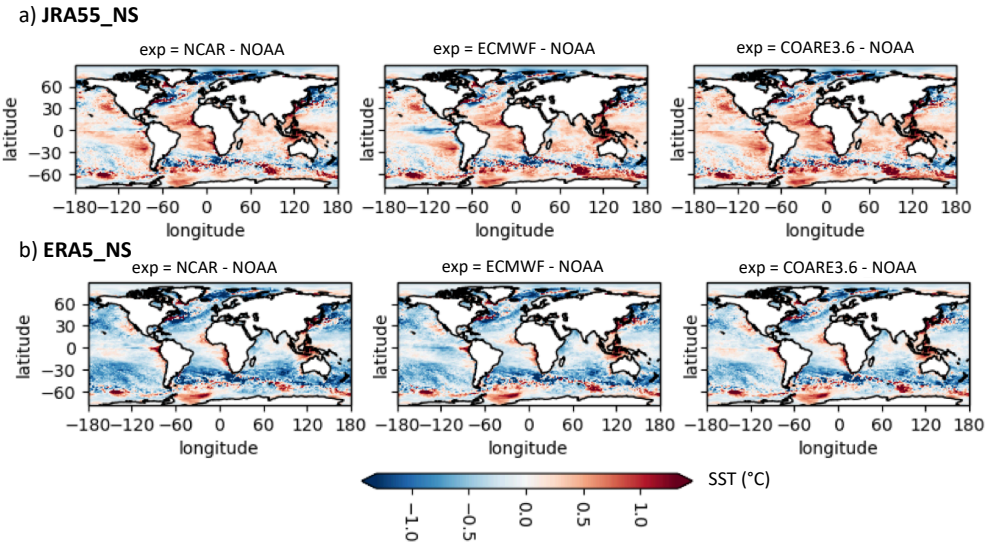

Figure 3: Annual mean SST differences between JRA55_NS (a) and ERA5_NS (b) set of experiments (NCAR, ECMWF and COARE3_6, From left to right) and NOAA SST. Period: 2016-2018

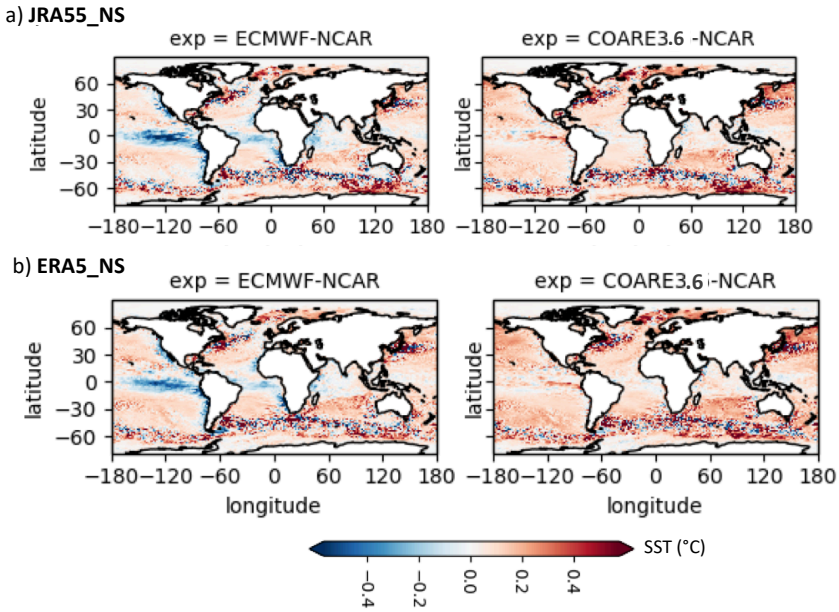

Figure 4: Annual mean SST differences among experiments (ECMWF-NCAR and COARE3_6 - NCAR, from left to right) for JRA55_NS (a) and ERA5_NS (b). Period: 2016-2018

SKIN TEMPERATURE (ERA5_NS VS ERA5_S)

The SST differences among experiments, which differ only for the bulk used to compute the air-sea fluxes, result forcing independent (Figure 4). ECMWF SST field present colder sea surface temperature than NCAR and COARE3.6 SST over EBUS and tropical Pacific and Atlantic. ECMWF and COARE3.6 algorithms are meant to be used with the skin temperature (SSST or Ts) instead of the SST. The skin temperature, as Figure 5 show for ECMWF (Figure 5a) and for COARE3.6 (Figure 5b) algorithm, is colder than SST of $0.3°C$ on average. Therefore, the use of the CSWL scheme to calculate the flux may substantially reduces the evaporation and total turbulent heat flux QT (i.e., QL + QH), likely mitigating the cold temperature differences reported in Figure 4. In this section we compare results from ERA5_S set of experiments, which is conducted using the CSWL scheme and ERA5_NS. In Figure 6, as expected, SST differences between ERA5_S and ERA5_NS (e.g. SKIN-NOSKIN) results positive for both ECMWF (Figure 6a) and COARE3.6 (Figure 6b) bulk formulae, with a maximum values of $0.3°C$ over the western equatorial Pacific, the Indo-Pacific Warm Pool. In the tropical eastern Pacific, in the Northen Pacific and in the Southern ocean the differences are weaker than $0.1°C$. The discrepancies among algorithms noted in the previous section (e.g. colder temperature in Pacific and Atlantic tropics for ECMWF experiment, Figure 4) are not, therefore, explained by the implementation of the CSWL scheme. The patterns of errors with respect to observation (Figure 7) reflect the differences between ERA5_S and ERA5_NS. Specifically, the cold differences between ERA5_NS and NOAA (NOSKIN - NOAA, Figure 7 right panels) result dumped in ERA5_S differences with NOAA (SKIN-NOAA, Figure 7 left panels), while the warm differences between ERA5_NS and NOAA result amplified. This is due to the overall warming of the ocean in the ERA5_S set of experiments with respect to ERA5_NS (Figure 6). Overall no significant changes are evident for both set of experiments (see Figure 7).

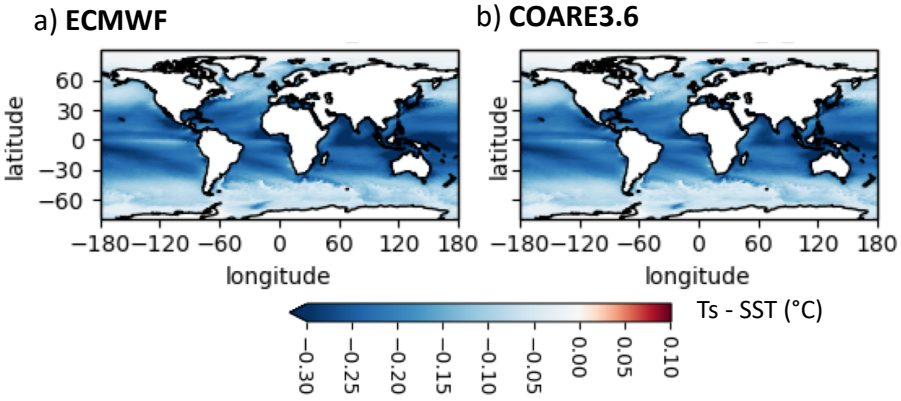

Figure 5: Annual mean temperature difference between the surface skin temperature Ts and the SST for COARE3.6 (calculated from ERA5_6_COARE3.6 experiment) and ECMWF (calculated from ERA5_S_ECMWF experiment) algorithms. Period: 2016-2018

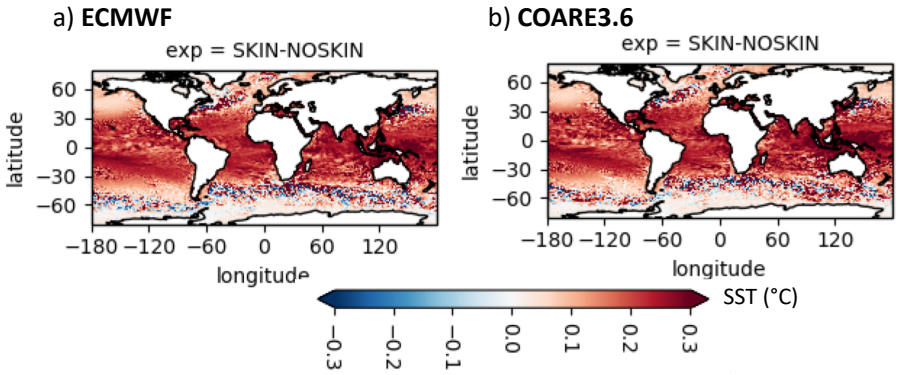

Figure 6: Annual mean SST differences between ERA5_S set of experiments and ERA5_NS set of experiments for ECMWF (a) and COARE3.6 (b) algorithms. Period: 2016-2018

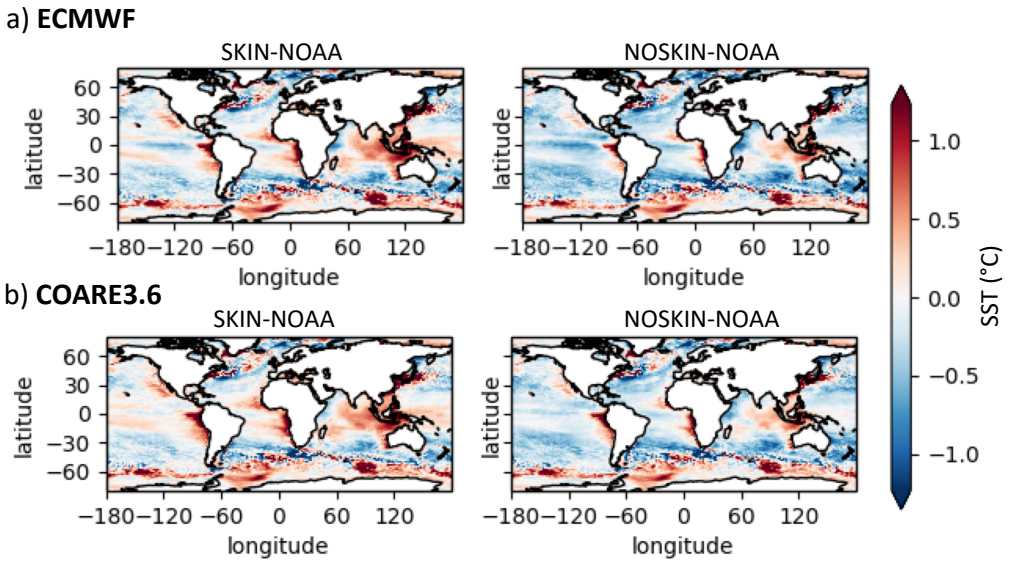

Figure 7: Annual mean SST differences between SKIN set of experiments (left column) and NOAA SST (e.g. SKIN-NOAA) and between NOSKIN set of experiments and NOAA SST (e.g. NOSKIN-NOAA) for ECMWF(a) and COARE3.6 (b) algorithms. Period: 2016-2018

SEASONAL SEA SURFACE TEMPERATURE IN ERA5_S SET OF EXPERIMENTS

As we presented in the previous subsections, the differences between bulk algorithms in driving the SST pattern are not related neither to the forcing or to the CWSL scheme temperature . In this subsection we examine, for each season, ERA5_S set of experiments. Target season is then selected to study in details the possible drivers of the ocean response. Figure 8 shows mean seasonal SST differences between ERA5_S experiments (e.g. NCAR, ECMWF and COARE3.6)

and NOAA SST, while Figure 9 shows SST differences among experiments. In comparison with observation all the algorithms show similar patterns through the seasons. Winter presents the most intense warm bias in the Southern Hemisphere, especially along eastern tropical Pacific (up to $2°C$). Spring, Fall and Summer show similar patterns of differences: warm biases along EBUS and cold bias over Southern Ocean and Equator. More interesting are, instead, the differences among experiments (Figure 9). Overall ECMWF and COARE3.6 are warmer than NCAR experiment due to the implementation of the skin temperature (compare Figure 9 with Figure 4b). ECMWF experiment shows the peculiar colder temperature along tropical Pacific and along EBUS which varies through the seasons. The SST difference signature is intense during Summer and Fall with a peak in Spring, while is almost dumped during winter season. Spring season, due to its different results on SST pattern in ECMWF algorithm, is selected to investigate the possible drivers that determine the ECMWF peculiar ocean response. Equatorial Pacific and EBUS are regions dominated by wind driven upwelling (e.g. ekman pumping and coastal upwelling), therefore, we investigate the wind stress forcing differences between ERA5_S experiments. Referring to Equation 1a, bulk formula establishes wind stress as a function of the wind speed vector at height z (u_z), of the scalar wind speed $|u_z|$ with the potential inclusion of a gustiness contribution (u) and of the wind transfer coefficient (C_D). Figure 10 show for ERA5_S mean fields (left column, only NCAR mean fields are shown as reference) and differences among experiments (right column) for u, C_{DN} and C_D. The scalar wind differences are related to the inclusion of the gustiness in the bulk calculation for ECMWF and COARE3.6. The gustiness correction prevent bulk formulas error when wind speed approaches zero (e.g in calm conditions). The differences between experiments do not exceed 0,5 m/s and they are located along calm condition areas (wind speed < 5m/s, see Figure 10a), such as north of tropical band ($5°N - 10°N$), and over sea-ice covered regions (e.g. nearby Antarctica during spring). More interesting are the patterns related to the transfer coefficients. C_D and C_{DN} differences between experiments show similar patterns (compare Figure 10b with 10c), suggesting that the differences in C_D momentum transfer coefficient are related to the neutral coefficient (C_{DN}) calculation rather than to its stability correction (term to add to C_{DN} to get C_D coefficients). This is confirmed by the differences between C_D and C_{DN} (Figure 11). The pattern of differences (C_D - C_{DN}) for each experiment is really similar among experiments, likely due to the fact that all the algorithms use the same stability empirical function (see bulk algorithms in section). $C_D - C_{DN}$ pattern is positive in regions dominated by unstable condition, tropical band, and sea-ice covered areas and negative in atmospheric stable regions (e.g. Arctic ocean during no sea-ice season, spring).

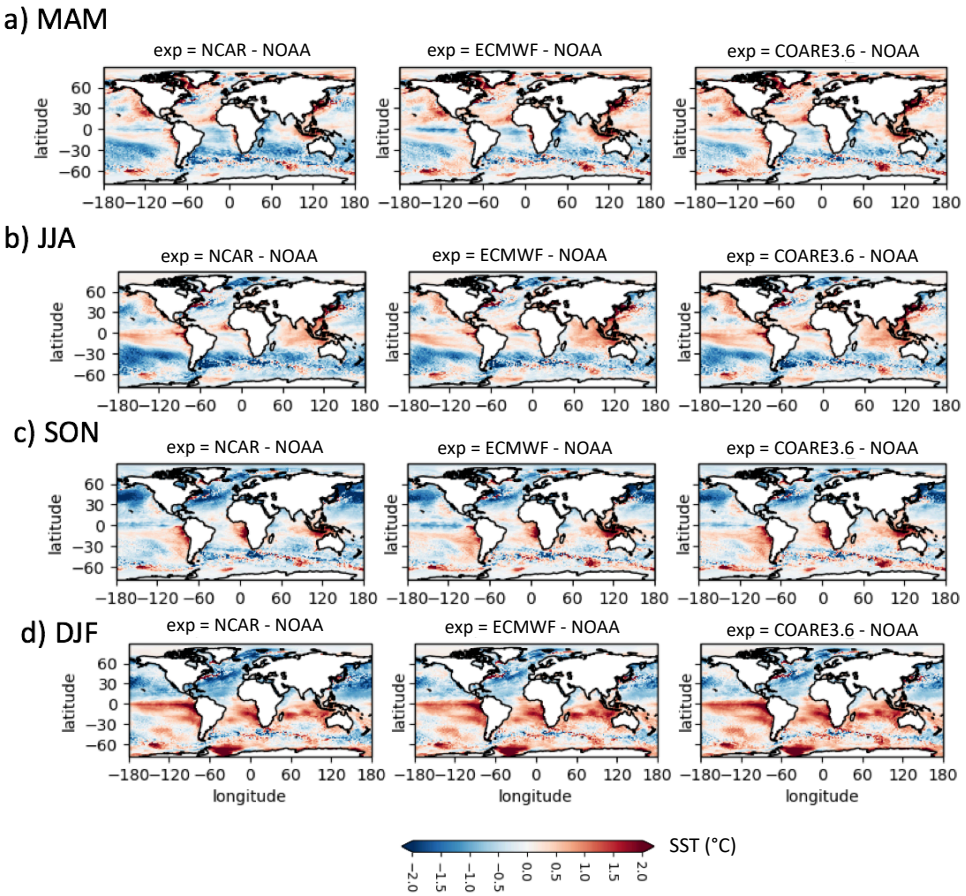

Figure 8: Mean SST differences between ERA5_S set of experiments (NCAR, ECMWF and COARE3.6 from left to right and NOAA SST for MAM (a) JJA (b), SON (c), DJF (d) seasons. Period: 2016-2018

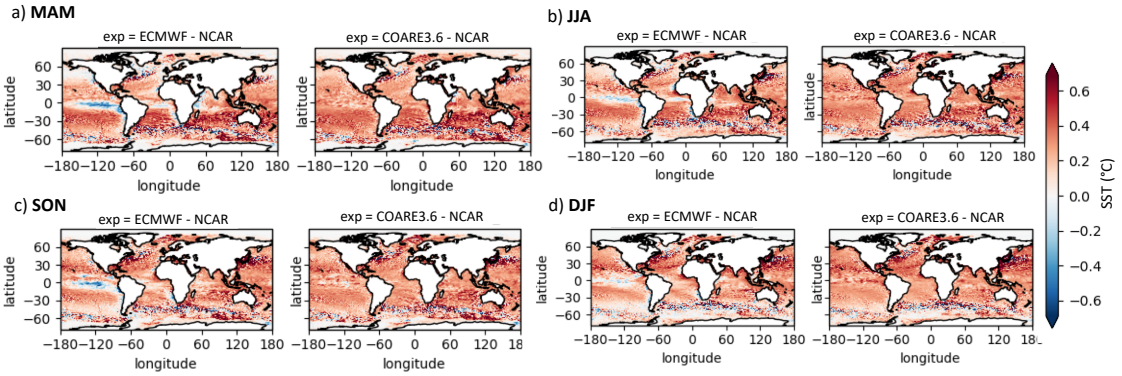

Figure 9: Mean SST differences among ERA5_S set experiments (ECMWF-NCAR and COARE3.6 - NCAR, from left to right) for MAM (a) JJA (b), SON (c), DJF (d) seasons. Period: 2016-2018

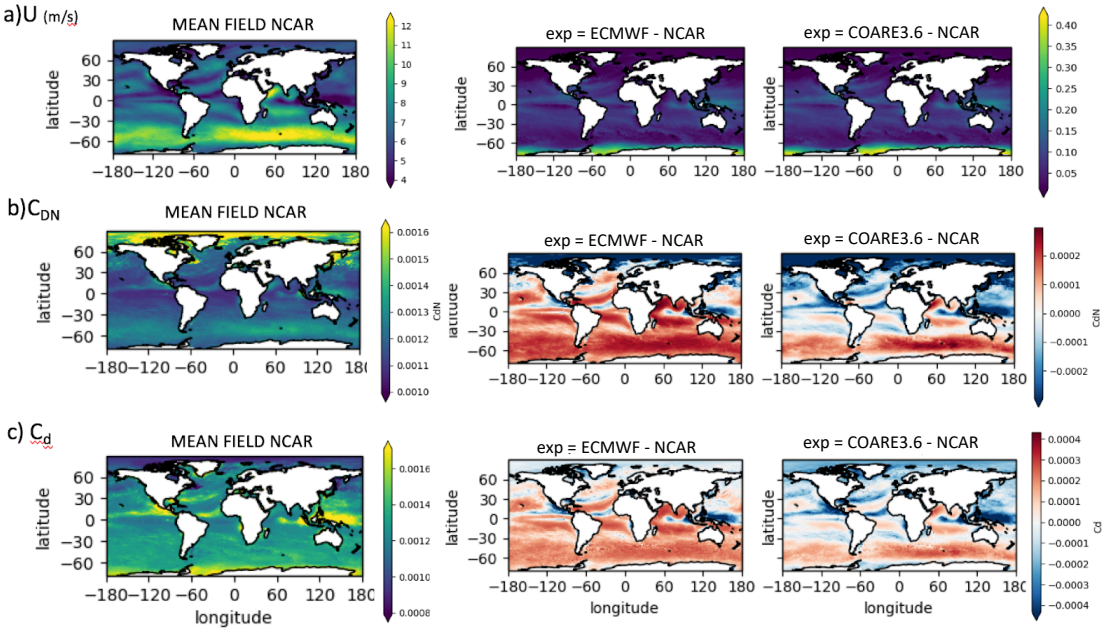

Figure 10: MAM mean of ERA5_S_NCAR experiment (left column) and differences among ERA5_S set experiments (ECMWF-NCAR and COARE3.6 - NCAR, right columns) for scalar wind speed U (a) , for neutral momentum transfer coefficient C_{DN} (b) and for momentum transfer coefficient C_D (c) . Period: 2016-2018.

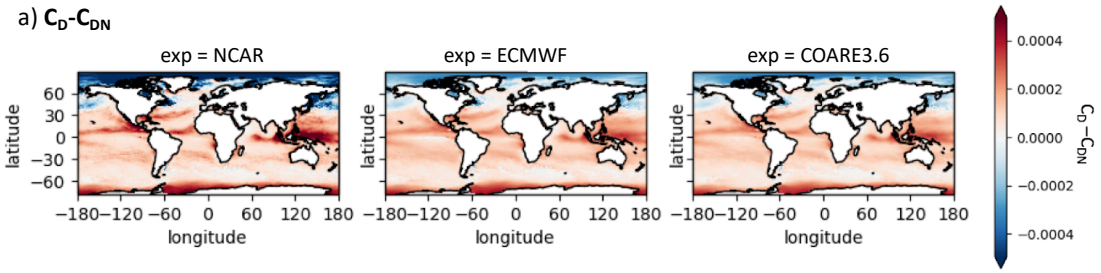

Figure 11: Mean $C_D - C_{DN}$ differences for ERA5_S set of experiments (NCAR, ECMWF and COARE3.6 from left to right) for MAM season. Period: 2016-2018

u and C_D differences among experiments (Figure 10a-c) explain the resulting different fields after bulk calculation (e.g. τ, τ_y, τ_x, Figure 12a-b-c). In particular, for wind speeds above $5m/s$ (Figure 10a), the C_D of COARE3.6 and, in particular the ECMWF C_D, are larger than NCAR C_D. This leads to a substantial increase of the wind stress over the ACC, over northern midlatitudes (e.g. EBUS), and Atlantic storm for ECMWF experiment and, with lower extent, for COARE3.6 experiment (Figure 12a). On the other hand, from calm up to light breeze conditions ($u < 5m/s$), the C_D of NCAR is larger than that COARE3.6 C_D and to lower extend to ECMWF C_D. These conditions occur quite frequently north of the tropical band during spring ($5°N - 10°N$). The differences lead to a slightly decrease of the wind stress in these areas for ECMWF experiment and to a substantial decrease of wind stress for COARE3.6 experiment (Figure 12a). Note that the wind stress differences are only amplitude deviation from the mean field (e.g. wind stress directions are coherent among the experiments). Different is the hypothesis for the ECMWF Pacific and Atlantic equatorial cold SST difference (Figure 9). The pattern of wind stress curl in the tropics during Spring (Figure 13) is dominated by a band of positive curl along $5°N - 10°N$ where the northeast trades build to the north, and a narrow strip of positive curl just north of the Equator sustained by the lateral gradient of wind stress generated by the acceleration of southeast trades surface winds over the northern front of the equatorial cold tongue (Chelton et al., 2001, [17]) accompanied by a more extended band of negative curl to the south. The stronger southeast trades compared to NCAR and COARE3.6 experiment over the equatorial cold tongue ($5°S - 5°N$) in ECMWF experiment (Figure 12b) is bound to result in stronger convergence (and negative stress curl via the lateral gradient of wind stress, Figure 13) when crossing the southern SST front and form a strip of divergence (with a thin strip of positive curl, Figure 13) when crossing over the northern SST front (Chelton et al., 2001, [17]). Stronger positive curl north of equator and stronger negative curl south of equator likely enhance ekman pumping along the equatorial cold tongue in ECMWF experiment. Therefore, stronger ECMWF meridional wind stress along EBUS with respect to NCAR and COARE3.6 experiments could favor coastal upwelling explaining the SST differences over EBUS.

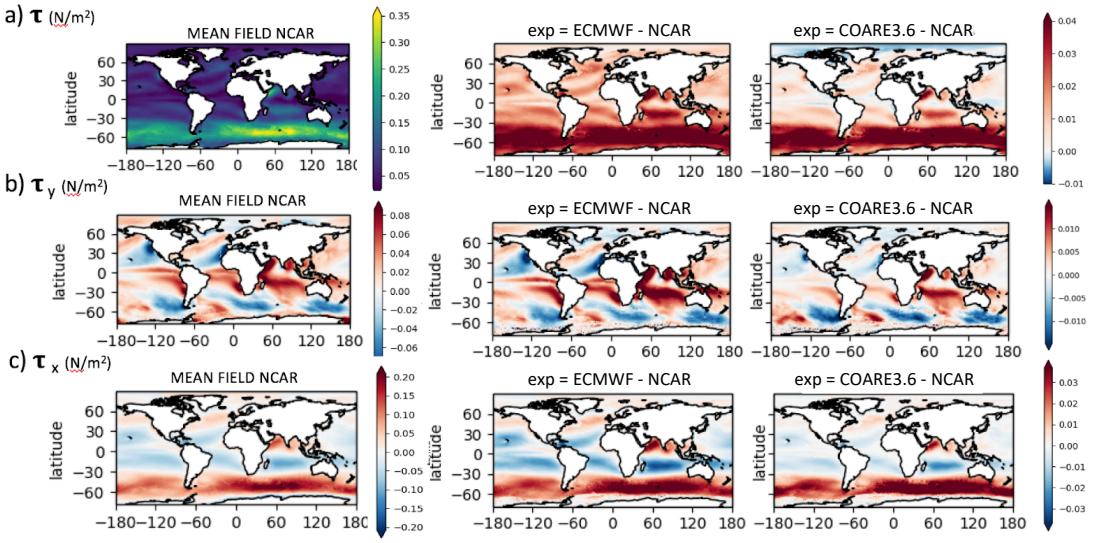

Figure 12: MAM mean of ERA5_S_NCAR experiment (left column) and differences among ERA5_S set experiments (ECMWF-NCAR and COARE3.6 - NCAR, right columns) for wind stress module τ (a) , for meridional wind stress τ_y (b) and for zonal wind stress τ_xc) . Period: 2016-2018.

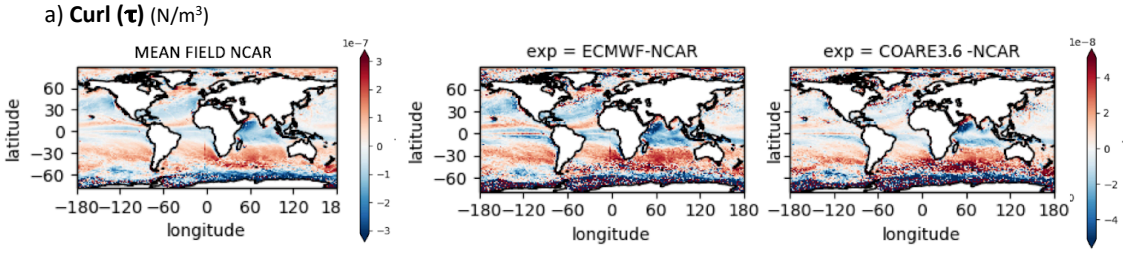

Figure 13: Wind stress curl mean, curl(τ), of ERA5_S_NCAR experiment (left column) and differences among ERA5_S set of experiments (ECMWF-NCAR and COARE3.6 - NCAR, right columns) for MAM season. Period: 2016-2018.

4. CONCLUSIONS AND FUTURE PERSPECTIVES

This report presents a review of the bulk formulation available in last release of the NEMO ocean model (v.4, revision 050) and discusses their impacts on the sea surface temperature. To provide surface boundary conditions to the ocean, NEMO can use three different bulk algorithms, namely NCAR , ECMWF and COARE3.6. There are substantial differences among the mentioned bulks, both in their theoretical formulation and in the effect on the ocean surface properties. Table 1

summarizes the principal differences among algorithms: skin surface temperature and convective gustiness are used in COARE3.6 and ECMWF algorithms, while NCAR uses SST and the zero wind singularity is avoided by simply setting a minimum value for the scalar wind speed of 0.5 m/s. Furthermore, ECMWF and COARE3.6 parametrize the roughness lengths, using Charnock parameter, while in NCAR the three neutral BTCs are empirical functions of U_{N10}. Lastly, the coefficients of the stability empirical function are the same for ECMWF and NCAR, while COARE3.6 adopts slightly different coefficients. In terms of ocean response, our sensitivity tests show that ECMWF simulates a colder SST compared to NCAR and COARE3.6 over the EBUS and equatorial Pacific and Atlantic sectors, with a difference up to $0.6°C$. We find that the bulk-formulation differences in driving the SST pattern are not related neither to the atmospheric forcing or to the CWSL scheme temperature. Analysis of wind transfer coefficients and wind stress differences suggests a significant role of the wind stress in shaping the SST pattern. Likely, stronger ECMWF meridional wind stress along EBUS and stronger curl over Pacific and Atlantic tropical band with respect to NCAR and COARE3.6 experiments might drive the SST differences. Further investigation is needed to understand the complete response of the upper ocean to the bulk formulations and select the best set-up for global model application. For this purpose, a set of idealized experiments will be performed modifying the bulk formulation, for example using mixed transfer coefficient (C_D, C_q and C_t from different bulk algorithms).

Bibliography

[1] NEMO System Team. *NEMO ocean engine*.

[2] Harald Ulrik Sverdrup, Martin Wiggo Johnson, Richard H Fleming, et al. *The Oceans: Their physics, chemistry, and general biology*, volume 7. Prentice-Hall New York, 1942.

[3] John A Goff. Saturation pressure of water on the new kelvin temperature scale. *Transactions of the American society of heating and ventilating engineers*, pages 347–354, 1957.

[4] Laurent Brodeau, Bernard Barnier, Sergey K Gulev, and Cian Woods. Climatologically significant effects of some approximations in the bulk parameterizations of turbulent air–sea fluxes. *Journal of Physical Oceanography*, 47(1):5–28, 2017.

[5] James B Edson, Venkata Jampana, Robert A Weller, Sebastien P Bigorre, Albert J Plueddemann, Christopher W Fairall, Scott D Miller, Larry Mahrt, Dean Vickers, and Hans Hersbach. On the exchange of momentum over the open ocean. *Journal of Physical Oceanography*, 43(8):1589–1610, 2013.

[6] WoG Large and SG Yeager. The global climatology of an interannually varying air–sea flux data set. *Climate dynamics*, 33(2-3):341–364, 2009.

[7] ECMWF. *Part III: Dynamics and Numerical Procedures*. Number 3 in IFS Documentation. ECMWF, 2015. Operational implementation 12 May 2015.

[8] Andreĭ Monin. Basic laws of turbulent mixing in the surface layer of the atmosphere.

[9] Charles Pelletier, Florian Lemarié, and Eric Blayo. Sensitivity analysis and metamodels for the bulk parametrization of turbulent air–sea fluxes. *Quarterly Journal of the Royal Meteorological Society*, 144(712):658–669, 2018.

[10] Stuart D Smith. Coefficients for sea surface wind stress, heat flux, and wind profiles as a function of wind speed and temperature. *Journal of Geophysical Research: Oceans*, 93(C12):15467–15472, 1988.

[11] Anton CM Beljaars. Air–sea interaction in the ecmwf model. In *Proc. Seminar on Atmosphere–Surface Interaction*, pages 33–52, 1997.

[12] Eric B Kraus and Joost A Businger. *Atmosphere-ocean interaction*. Oxford University Press, 1994.

[13] Hiroyuki Tsujino, Shogo Urakawa, Hideyuki Nakano, R Justin Small, Who M Kim, Stephen G Yeager, Gokhan Danabasoglu, Tatsuo Suzuki, Jonathan L Bamber, Mats Bentsen, et al. Jra-55 based surface dataset for driving ocean–sea-ice models (jra55-do). *Ocean Modelling*, 130:79–139, 2018.

[14] Hans Hersbach. The era5 atmospheric reanalysis. *AGUFM*, 2016:NG33D–01, 2016.

[15] Copernicus Climate Change Service (C3S). Era5: Fifth generation of ecmwf atmospheric reanalyses of the global climate. 2017.

[16] Richard W Reynolds, Thomas M Smith, Chunying Liu, Dudley B Chelton, Kenneth S Casey, and Michael G Schlax. Daily high-resolution-blended analyses for sea surface temperature. *Journal of Climate*, 20(22):5473–5496, 2007.

[17] Dudley B Chelton, Steven K Esbensen, Michael G Schlax, Nicolai Thum, Michael H Freilich, Frank J Wentz, Chelle L Gentemann, Michael J McPhaden, and Paul S Schopf. Observations of coupling between surface wind stress and sea surface temperature in the eastern tropical pacific. *Journal of Climate*, 14(7):1479–1498, 2001.

[18] WG Large and S Pond. Sensible and latent heat flux measurements over the ocean. *Journal of physical Oceanography*, 12(5):464–482, 1982.